# CONGENITAL CARDIOLOGY TODAY

News and Information for Pediatric and Congenital Cardiovascular Physicians and Surgeons

Vol. 4 / Issue 7
July 2006
North American Edition

WWW.CONGENITALCARDIOLOGYTODAY.COM


INSIDE THIS ISSUE


**Energy-Depleting Fluid-Flow Disturbances Associated with Small Pressure Change: Relevance to Obstructed Total Cavopulmonary Connections**
*by Joshua P. Wiesman, MS; Donald P. Gaver, PhD; Nancy T. Ross-Ascuitto, MD; and Robert J. Ascuitto, PhD, MD*
~Page 1

**The World Loses a Gifted Pediatric Cardiologist, Pathologist, and Philosopher**
*by Richard Van Praagh, MD*
~Page 12

**Searching For and Mending Broken Hearts in Mongolia**
*by Kirk A. Milhoan, MD, PhD; Kimberly D. Milhoan, MD; Ariuntsatsral Erdenebileg, MD*
~Page 13



CONGENITAL CARDIOLOGY TODAY
9008 Copenhaver Drive, Ste. M
Potomac, MD 20854 USA
Tel:+1.301.279.2005
Fax: +1.240.465.0692
www.CongenitalCardiologyToday.com





See recruitment ad on page 11


**Congenital Cardiology Today would like to share your interesting stories or research in congenital cardiology.**

Submit a brief summary of your proposed article to

**Article-July@CCT.bz**

# ENERGY-DEPLETING FLUID-FLOW DISTURBANCES ASSOCIATED WITH SMALL PRESSURE CHANGE: RELEVANCE TO OBSTRUCTED TOTAL CAVOPULMONARY CONNECTIONS


*By Joshua P. Wiesman, MS; Donald P. Gaver, PhD; Nancy T. Ross-Ascuitto, MD; and Robert J. Ascuitto, PhD, MD*



## Abstract

Flow-energy dissipation reduces hemodynamic efficiency of a Total Cavopulmonary Connection (TCPC), or Fontan-modified circulation. Anatomical obstructions within the systemic venous-to-pulmonary arterial pathway are often associated with small (<1 mmHg) measured pressure changes. Nevertheless, the associated flow disturbances can give rise to prominent alteration in flow velocity, an important determinate of energy loss. We used a computer-based description of non-pulsatile fluid flow through a conduit taken to simulate blood traversing a narrowed portion of a Fontan cavopulmonary passage. Fluid pressure distributions and flow-velocity fields were determined from numerical solutions (finite element analysis) of the Navier-Stokes equations for the flow transitions. Our findings indicate significant fluid energy loss for flow ($1.65*10^{-5}$ $m^3/s$ or 1L/min) crossing wedge-like or circumferential obstructions, each chosen to produce a 40% reduction in conduit cross-sectional area. Pressure drops were calculated, and found to average only ~ 26.7 $N/m^2$ or ~ 0.2 mmHg. Despite these small pressure changes, prominent regions of flow stagnation and flow reversal were identified distal to the obstructions. By analogy, the consequence such flow patterns may have on perfusion through TCPCs is discussed. Based on our analysis, a treatment strategy in caring for post-Fontan patients would be to optimize cavopulmonary blood flow pathways to obliterate flow disturbances, thereby helping to conserve flow energy.


## Introduction

The Total Cavopulmonary Connection (TCPC), commonly referred to as the Fontan procedure, has become the surgical treatment of choice for children with functional single-ventricle heart disease [1-3]. The TCPC entails creating direct superior and/or inferior vena cava-to-pulmonary artery tubular connections that channel blood flow directly to the lungs [4-6]. An important factor governing successful hemodynamic performance following Fontan completion is the capacity of the surgically-crafted cavopulmonary pathway to conserve the traversing blood

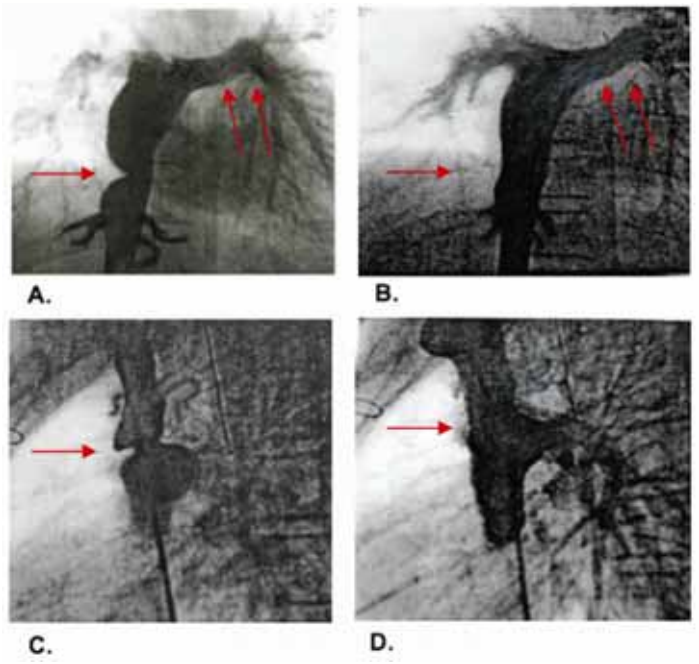


*Figure 1 (A - D): Clinical examples of obstructed portions of Fontan cavopulmonary pathways. (A) Angiogram showing the inferior vena cava-to-pulmonary artery pathway in a patient having undergone surgical palliation for hypoplastic left heart syndrome. A wedge-like obstruction is seen occluding the intracardiac conduit at the level of the diaphragm (arrow). Early systemic venous collaterals can be seen proximal to the obstruction. An approximately 0.3 mmHg pressure drop was measured across the obstruction by direct pullback; the distal conduit mean pressure was 12 mmHg. Pressure measurements were performed using a Phillips, Mac-Lab 7000 System. Pressure tracings were recorded on scale 0-to-20 mmHg using 41 reference gridlines. Note the previously placed intravascular stent in the proximal left pulmonary artery (double arrow). (B) Angiogram showing the intracardiac conduit to be widely patent after placement of an (18-26 mm) x 26 mm balloon-mounted intravascular stent (Intra Therapeutics, St Paul, MN). No residual pressure drop was detected across the newly stented region. (C) Angiogram showing the superior vena cava-to-right pulmonary artery pathway in a patient having undergone surgical palliation for hypoplasia of the right ventricle, ventricular septal defect and straddling tricuspid valve. A circumferential ridge of tissue is seen constricting the bidirectional Glenn anastomosis (arrow). Early systemic venous collaterals can be seen proximal to the obstruction. An approximately 0.4 mm Hg pressure drop was measured across the obstruction by direct pullback; the right pulmonary artery mean pressure was 12 mmHg. Same pressure recording system as in (A). (D) Angiogram showing the anastamosis site to be widely patent after dilatation with a (14 mm x 20 mm) balloon catheter (XXL. Boston, MA). No residual pressure drop was detected across the ballooned region.*

flow's motional energy. Therefore, anatomical configurations depleting energy from the flow, such as those producing acute change in pathway size – either larger or smaller [7-9] – and/or direction [7-8], can severely reduce efficiency of the Fontan circulation.

In post-Fontan patients, cardiac catheterization is often employed to help delineate abnormalities within the cavopulmonary system that may impede pulmonary blood flow. Since there is so little ventricular *vis a tergo* in a TCPC, flow is largely passive, and of low velocity. Therein, a clinically measurable pressure change across a suspected, or angiographically identified, obstruction often is quite small (< 1 mm Hg), see Fig. 1. Nonetheless, the associated hemodynamic disturbance can give rise to prominent alteration in flow velocity (both in magnitude and direction), a critical determinant of fluid energy loss.

The purpose of this investigation is to employ a computation-based description of non-pulsatile fluid flow through a conduit, chosen to simulate blood crossing an obstructed portion of a Fontan cavopulmonary pathway. Two anatomical forms of obstruction are considered. The first is a wedge-like occlusion, Figs. 1A and 2a, and the second a circumferential constriction, Figs. 1C and 2b. Both types of obstructions were taken to have the same cross-sectional area for flow. We postulated, under systemic venous perfusion conditions, energy-depleting flow disturbances can be created, even with minimal overall pressure loss, as a consequence of fluctuating fluid pressure and re-distribution of flow velocity in the region of obstruction. Using pressure distributions and velocity fields determined from numerical solutions (using finite element analysis) to the Navier-Stokes equations for the proposed flow transitions, pressure recovery and flow energy losses were assessed along the downstream fluid pathway. Regions of flow stagnation and flow reversal are identified. By analogy, the clinical consequence such flow patterns may have for effective perfusion through TCPC's are discussed.

**Rational**

In our model, incompressible, non-pulsatile fluid flow through a conduit was considered to satisfy the energy-balance equation:

(1) $$\Delta W_{i,f} = \left( < P >_i + \frac{\rho}{2} < V^2 >_i \right) Q_i - \left( < P >_f + \frac{\rho}{2} < V^2 >_f \right) Q_f .$$

The quantity $\Delta W_{i,f}$ represents the energy dissipated per time or power loss for the flow transition ($i$ to $f$). The subscripts ($i$) and ($f$) designate the initial (or incoming) and final (or outgoing) portions of the fluid pathway, respectively. Rho ($\rho$) is the fluid density and Q the flow rate. The terms $<P>$ and $\frac{\rho}{2} < V^2 >$ represent flow-averaged pressure ($P$) and kinetic energy ( $\frac{\rho}{2} V^2$ ) respectively, where:

(2A) Pressure $$< P >= \frac{1}{Q} \int_A p dq$$

(2B) Kinetic Energy $$\frac{\rho}{2} < V^2 >= \frac{1}{Q} \int_A \frac{\rho}{2} v^2 dq$$

(2C) Flow Rate . $$Q = \int_A dq .$$

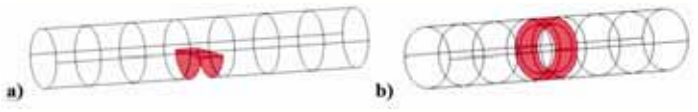


*Figure 2. Schematic representation of a cylindrical conduit used to computationally describe fluid flow across a wedge-like (a) and circumferential (b) obstruction (shaded regions). The shaded areas represent 40% of the unobstructed conduit's cross-sectional area.*

Here $p$ and $v$ denote the local pressure and magnitude of the velocity ($v$) associated with flow ($dq$) crossing a differential area ($da$). The elemental flow satisfies $dq = v_N\, da$, where $v_N$ is the velocity component normal to $da$. The symbol $\left(\int_A\right)$ designates the summation (weighted by the flow) or integration (with respect to the flow) of $p$ and $\frac{\rho}{2}v^2$, as flow is distributed over the conduit's cross-sectional area ($A$). In general, the pressure distributions and velocity fields will be dissimilar over $A_i$ and $A_f$. Thus, the corresponding bracketed terms $<>_i$ and $<>_f$, in Eq. (1), which are to be evaluated over the entrance and exit areas $A_i$ and $A_f$, respectively, will take on different values. Equation (2A) reflects the rate pressure force performs work on fluid crossing ($A$); Eq. (2B) designates the rate kinetic energy is carried by fluid crossing ($A$). The quantity $\Delta W_{i,f}$ may further be written as $\Delta E_{i,f}\, Q_f$, where the flow energy loss term $\Delta E_{i,f}$ describes the power loss of the fluid system per unit of fluid flow. The pressure contribution to $\Delta E_{i,f}$ is:

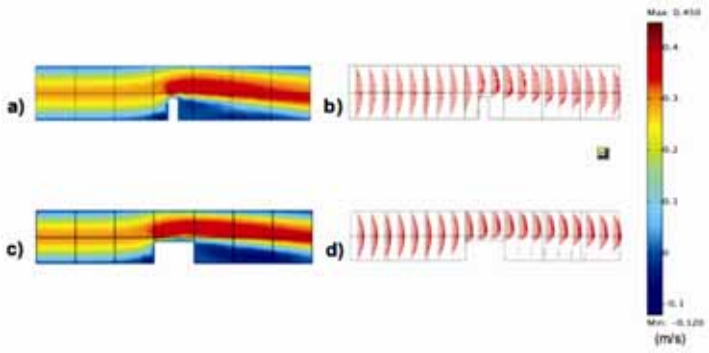


*Figure 3. Color-coded flow-velocity, in m/s, distributions (a and c) and flow-velocity profiles (b and d) characterizing fluid crossing wedge-like obstructions of length 0.002 m and 0.01 m. The orange segments indicate regions of increased fluid velocity arising as a consequence of the flow traversing the narrowed segment of the conduit. The dark-blue areas designate adjacent regions of flow stagnation and flow reversal. Note flow's contracted velocity profile as it emerges from the obstruction and propagates downstream. Short obstructions result in smaller stagnation regions distal to the obstruction.*

(3A) $$(\Delta E_{i,f})_P = (\,<P>_i - <P>_f\,)$$

The kinetic energy contribution to $\Delta E_{i,f}$ is:

(3B) $$(\Delta E_{i,f})_{KE} = \left(\frac{\rho}{2}<V^2>_i - \frac{\rho}{2}<V^2>_f\right).$$

Note, $(\Delta E_{i,f})_{KE}$, will be negative when the flow's final kinetic energy exceeds its initial kinetic energy, as occurs when flow undergoes contraction. These quantities combine to form the flow energy loss term, $\Delta E_{i,f}$, for the fluid system:

(3C) $$\Delta E_{i,f} = (\,\Delta E_{i,f}\,)_P + (\,\Delta E_{i,f}\,)_{KE}$$

Equation (3C) may be re-arranged to read as follows:

(3D) $$(\,\Delta E_{i,f}\,)_P = (\,\Delta E_{,f,i}\,)_{KE} + \Delta E_{i,f}$$

This form of Eq. (3C) shows that $(\Delta E_{i,f})_P$, which also represents the overall pressure change for the fluid transition, is determined by the change in flow kinetic energy and the flow energy loss. If pressure and flow-velocity are constant over $A_i$ and $A_f$, and energy dissipation is negligible, Eq (3D) reduces to the commonly-used form of the Bernoulli equation, $P_i + \frac{\rho}{2}V_i^2 = P_f + \frac{\rho}{2}V_f^2$. The various $\Delta Es$ represent energy per unit of fluid volume and thus carry equivalent units of pressure.

**Methodology**

The computational package FEMLAB 3.1 (Comsol, Inc., Burlington, MA) was used to create 3-dimensional models of non-pulsatile fluid flow through a rigid cylindrical conduit with a partial occlusion of length (L) (Figs. 2a and 2b). The conduit walls were assumed rigid because most surgically-constructed tubular passages are composed of non-compliant Gortex. The flow rate was fixed at a value, typical of that in a Fontan cavopulmonary pathway, namely $1.65*10^{-5}$ $m^3/s$ or 1L/min. Similarly, the pressure in the conduit distal to the

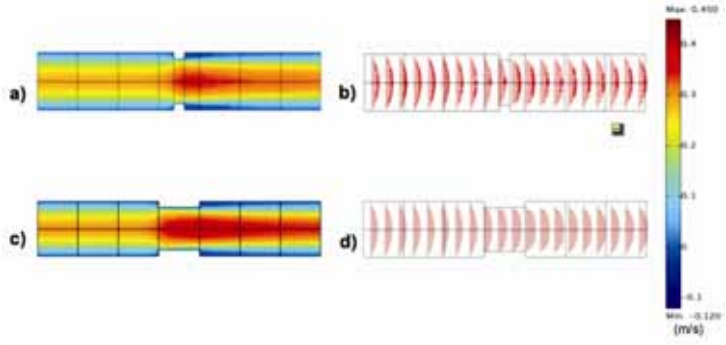


*Figure 4. Color-coded flow-velocity, in m/s, distributions (a and c) and flow velocity profiles (b and d) characterizing fluid crossing circumferential obstructions of length 0.002 m and 0.01 m. The orange segments indicate regions of increased fluid velocity arising as a consequence of flow traversing the narrowed segment of the conduit. The dark-blue areas designate concentric regions of flow stagnation. Note flow's contracted velocity profile, as it emerges from the obstruction and propagates downstream.*

obstruction was taken as a common value of 1600 N/m$^2$ or 12 mmHg, as for the examples in Fig. 1. The fluid pressure distributions and the flow velocity fields were determined along the conduit length in increments of 0.01m.

The accuracy of FEMLAB was assessed by first solving the problem of steady pipe flow (Poiseuille flow). The computer-generated overall pressure change between the ends of the pipe, flow axial velocity, flow rate and flow-induced wall shear stress were compared to corresponding values obtained from the exact analytical expressions for these quantities. The wall shear stress was determined to confirm that viscous contributions to fluid motion would be accurately assessed. The FEMLAB generated values were within 1% of the analytically-derived results. After confirming the accuracy of FEMLAB to solve the problem of non-obstructed Poiseuille flow, flow rate through a conduit containing an obstruction of length 0.005 m was calculated in 0.01m increments. Tracing the flow rate (conservation of mass), to within 1% of the predicted value, along both the unobstructed and obstructed portions of the conduit, verified that our numerical approach was of sufficient resolution to provide accurate results.

**Model Parameters**

A cross-sectional area and a length (L) defined the wedge-like and circumferential obstructions, as shown in Figs. 2a and 2b. The flow cross-sectional area was the same for both types of obstruction. The obstructions produced a 40% reduction in conduit cross-sectional area. Alternatively stated, the flow cross-sectional area was 60% of that for the unobstructed conduit. The length (L) was varied from that to produce thin (0.002 m) membrane-type obstructions to that for elongated (0.02 m) segments of narrowing. The remaining model parameters are as follows: conduit length = 0.07m, conduit diameter = 0.012 m, fluid density = 1050 Kg/m$^3$ and fluid viscosity = 3.5 x $10^{-3}$ N-s/m$^2$. The density and viscosity values were selected to allow blood to be treated as a Newtonian fluid. This transformation is valid since blood behaves as a Newtonian fluid under high rate-of-strain conditions, as occurs in the systemic venous system. The reader wishing to skip over the discussion of Numerical Analysis Techniques used for FEMLAB calculations may advance directly to the Results Section.

**Numerical Analysis Techniques**

The computer-simulated conduit consisted of domains combined to create the modeled vessel. The multi-domain construction technique allowed for greater flexibility in mesh resolution, a key element for accurate finite element analysis. For the wedge-like obstructions, the domain representing the conduit for the regions proximal to and distal to the interposed obstruction were described using the FEMLAB-defined "fine" mesh. The fine mesh entails a maximum element growth rate of 1.35, a maximum element size-scaling factor of 0.8, and curvature and cut-off factors of 0.35 and 0.008, respectively. The wall boundaries defining the region of obstruction required an "extra-fine" mesh, which decreases the element growth rate to 1.25, and the curvature and cut-off factors to 0.15 and 0.001, respectively. For the circumferential obstructions, the proximal and distal domains were described using the FEMLAB-defined "normal" mesh, while the region of obstruction again required the extra-fine mesh.

**Results**

Figures 3 and 4 compare color-coded flow-velocity distributions (a and c) and flow-velocity profiles (b and d) along the fluid pathway corresponding to the wedge-like (Fig. 2a) and circumferential (Fig. 2b) obstructions, of lengths 0.002m and 0.01m. The elongated orange segments emanating from the orifice of the obstructions signify higher values of fluid velocity arising as a consequence of flow having undergone contraction. The dark-blue areas along the walls of the conduit, distal to or in the shadow of the obstructions, define regions of flow stagnation and flow reversal, which are particularly prominent for the wedge-like occlusions. These features are also reflected in the flow-velocity profiles. Both the velocity distributions and their respective profiles are consistent with a more contracted, or collimated, fluid stream beyond the elongated (0.01m) compared to the short (0.002 m) obstructions. Moreover, the downstream velocity profiles display delayed recovery to a distribution indicative of uniform flow (pre-obstruction pattern), for the elongated compared to the short obstructions, again the effect being more pronounced for the wedge-like occlusions.

Figures 5a and 5b show flow kinetic energy traces for the various obstruction lengths. These graphs describe the rate with which kinetic energy is carried by fluid crossing successive planes distal to the obstructions, i.e. $\int_A \frac{\rho}{2} v^3 dq$ from Eq 2B. In the absence of obstruction, there is no change in downstream kinetic energy (dashed line). However, kinetic energy steadily decreased with advancing dis-

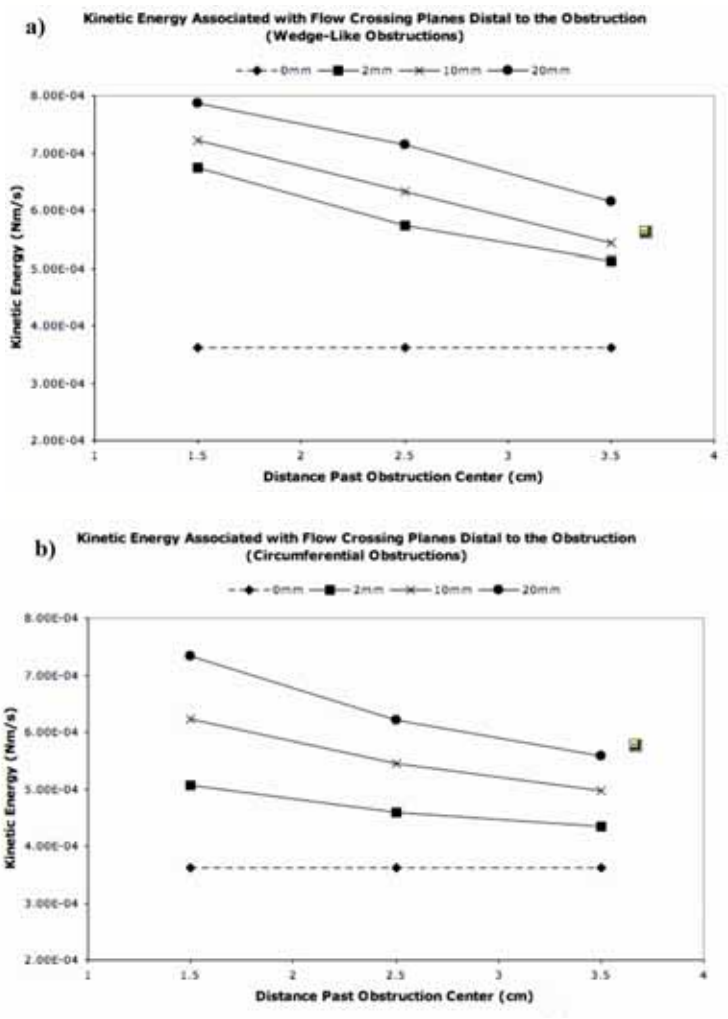


*Figure 5. Flow-kinetic energy traces, in Nm/s, i.e. calculated values of kinetic energy ($\int_A \frac{\rho}{2} v^3 dq$) associated with flow crossing successive planes distal to the wedge-like (a) and circumferential (b) obstructions of various lengths, 0, 2, 10, and 20 mm. Dashed line indicates absence of and solid lines presence of obstruction.*

tance beyond an obstruction (solid lines). Moreover, kinetic energy was higher for wedge-like compared to circumferential obstructions of the same length, and increased with increasing obstruction length. If one compares kinetic energies at equivalent distances from the orifice, rather than the center, of the obstructions, the kinetic energies continue to assume higher values for greater obstruction lengths (not shown).

The calculated overall pressure changes, $(\Delta E_{i,f})_P$, for the various transitions were greater for the wedge-like obstructions [ranging from 27.5 N/m$^2$ or 0.21 mmHg (L= 0.002 m) to 38.7 N/m$^2$ or 0.29 mmHg (L= 0.02 m), average ~ 32 N/m$^2$ or ~ 0.24 mmHg] compared to the circumferential obstructions [ranging from 16.8 N/m$^2$ or 0.13 mmHg (L= 0.002 m) to 28.1 N/m$^2$ or 0.21 mmHg (L= 0.02 m), average ~ 21.9 N/m$^2$ or ~ 0.16 mmHg]. The average pressure change characterizing all the transitions was ~ 26.7 N/m$^2$ or 0.2 mmHg. The pressure drops increased uniformly with obstruction length. The increase with respect to length was essentially the same for both types of obstructions, namely ~ 0.7 N/m$^2$/mm or ~ 0.005 mmHg/mm.

Figures 6a and 6b show fluid pressure traces. These graphs describe the average pressure exerted by fluid over successive planes distal to the obstructions, i.e. $\frac{1}{A}\int_A p da$. In the absence of obstruction, there is a minor decrease in downstream pressure (dashed line), as a consequence of the underlying viscous resistance to flow. For both types of obstructions, pressure increased (recovered) with advancing distance beyond the obstruction (solid lines). The final values approached the imposed constraint of a distal conduit pressure of 1600 N/m$^2$ or 12 mmHg.

Figure 7 shows color-coded representations of the quantity $(p v_N)$, associated with flow through a fluid pathway containing a wedge-like (a) and circumferential (b) obstruction. This quantity is used in the calculation of $< P >$, i.e. $\int_A p dq$ from Eq 2A. The distribution of $(p v_N)$ over the cross sectional area describes how the pressure $(p)$ and the axial component of flow velocity $(v_N)$ combine to transport energy to fluid flowing along the conduit. The orange segments denote energy contributions to forward flow and the dark-blue areas to reverse flow.

Figure 8a shows the overall percent increase in flow kinetic energy arising as a result of the transitions ($i$ to $f$). The gain

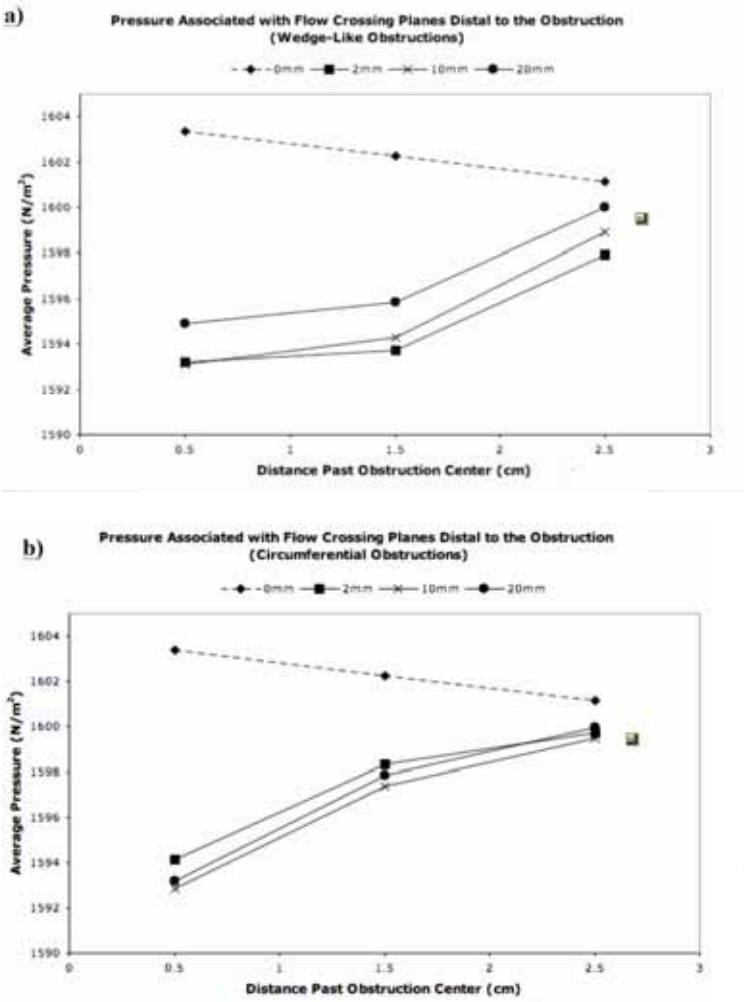


*Figure 6. Fluid pressure traces, in N/m$^2$, i.e. calculated values of average pressure* $(\frac{1}{A}\int_A pda)$ *over successive planes distal to the wedge-like (a) and circumferential (b) obstructions of various lengths, 0, 2,10, and 20 mm. Dashed line indicates absence of and solid lines presence of obstruction.*

in kinetic energy increased with increasing obstruction length, and was greater for wedge-like compared to circumferential obstructions of the same length. The flow kinetic energy contribution, $(\Delta E_{i,f})_{KE}$, to the energy loss term, $\Delta E_{i,f}$, is within a multiplicative factor the percent increase in kinetic energy. Thus, a plot of the magnitude of $(\Delta E_{i,f})_{KE}$ vs. obstruction length would be identical to that in Fig. 8a, except in overall scale. Figure 8b shows the corresponding energy loss term, $\Delta E_{i,f}$. Energy loss was greater (~ 50%) for wedge-like compared to circumferential obstructions of the same length, and increased with increasing obstruction length.

## Discussion

### *Features of TCPC Pathways*

Since its inception in 1971 [1], the Fontan operation for univentricular heart has undergone modifications directed at conserving cavopulmonary blood flow's motional energy in order to enhance pulmonary perfusion, minimize systemic venous pressure and decrease ventricular workload. Accordingly, de Leval et al. [4, 10] and Puga et al. [11] advocated a "Total Cavopulmonary Connection (TCPC)": the combination of a bidirectional Glenn shunt and an intracardiac conduit from the inferior vena cava to the right pulmonary artery. These groups postulated direct bicaval connections to the pulmonary arteries would result in more energy-sparing blood flow patterns. More recently, analytical [8-9, 12], empirical or in vitro [4, 13-18] and computer-based [10, 19-22] fluid-dynamics studies have suggested refinements of cavopulmonary connections, such as caval offsets [18], flaring of caval-to-pulmonary artery anastomosis sites [9], an extracardiac rather than an intracardiac conduit joining the inferior vena cava to the right pulmonary artery [16], etc., to further improve hemodynamic efficiency within the systemic venous portion of the Fontan circulation.

Nevertheless, several segments along the Fontan blood flow pathway remain at risk for developing obstruction. These portions include: the branch pulmonary arteries – especially the proximal left pulmonary artery due to compression by the neoaorta following Stage I of palliation for hypoplastic left heart syndrome (Fig. 1A), the superior vena cava-to-right pulmonary artery anastomosis (Fig. 1C), the portion of the inferior vena cava-to-right pulmonary artery intracardiac conduit at the level of the diaphragm (Fig. 1A), etc. Such obstructions within the cavopulmonary system may exacerbate effects associated with systemic venous hypertension, such as: hepatosplanchnic congestion, which can impair venous return from the gastrointestinal tract; and elevated superior vena cava pressure, which can restrict lymphatic resorption due to thoracic duct congestion. Both conditions have been implicated in protein losing enteropathy.

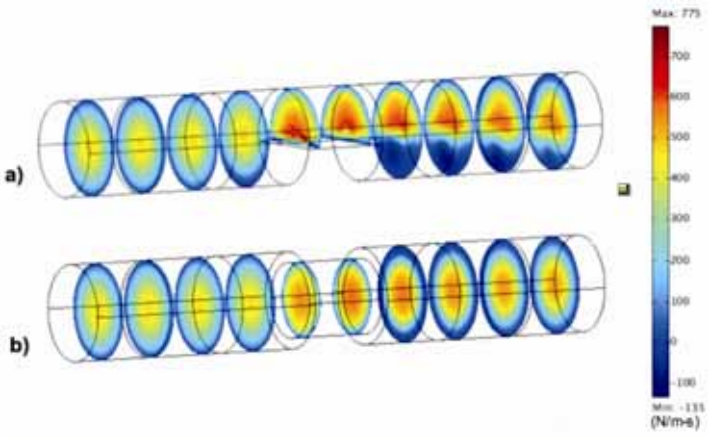


*Figure 7. Color-coded distribution of ( $pv_N$ ), in N/m-s, characterizing flow crossing successive planes along a fluid pathway containing a wedge-like (a) and a circumferential (b) obstruction. The orange segments depict the pressure-velocity contributions to forward flow and the dark-blue areas to reverse flow.*

### *Small Overall Pressure Changes Across Cavopulmonary Obstructions to Flow*

Cardiologists commonly use pressure gradient to assess severity of intravascular obstruction. However, in Fontan patients, pressure tracings obtained at cardiac catheterization often show minimal variation across the caval veins and the intracardiac conduit [15, 23-24], even in the presence of well-defined obstruction. Moreover, pressure assessment yields little information about flow velocity [22, 25-29], an important factor governing flow energy loss [7, 28]. Recently, it has been shown [7,28] that multidimensional phase-velocity magnetic resonance imaging can become an important tool for evaluating in vivo blood flow dynamics in Fontan patients, because flow velocity can be mapped along the systemic venous-to-pulmonary arterial pathway. The cases presented in Fig. 1 illustrate the typically low-pressure gradients (0.3-0.4 mmHg) encountered in angiographically-narrowed systemic venous pathways created by modified-Fontan procedures. The associated flow perturbations resulted in only an ~ 2% overall reduction in cavopulmonary pressure. Collateral venous communications between the caval veins may contribute to such small pressure losses. The azygous-lumbar venous system provides an extensive network of alternative channels for blood flow to bypass occlusions of the superior and/or inferior vena cava.

An important finding from our computational study is that for a passively perfused fluid system, taken to simulate blood flow through a stenotic portion of a Fontan systemic venous passage, obstructions causing marked re-distribution of flow velocity and significant energy dissipation, can be associated with small overall pressure changes [30]. For the flow transitions considered in this study, our calculated pressure drops averaged ~ 26.7 N/m$^2$ or ~ 0.2 mmHg, which constituted an ~ 2% decrease in conduit pressure. Although these pressure drops seem low, they are at least 3-fold higher than the pressure difference (0.06 mmHg) required to drive flow at 1 L/min through the unobstructed conduit, and more than 2-fold greater than the kinetic energy (0.09 mmHg) of the incoming fluid stream. These small transitional pressures largely reflect the low velocity of flow found in a cavopulmonary system.

In general, pressure drop across an obstruction is determined by the change in flow kinetic energy *and* the associated flow energy loss, Eq. (3D). In the absence of dissipative effects, the pressure drop *($\Delta P$)* can be estimated from the downstream kinetic energy using the simplified Bernoulli equation, i.e.

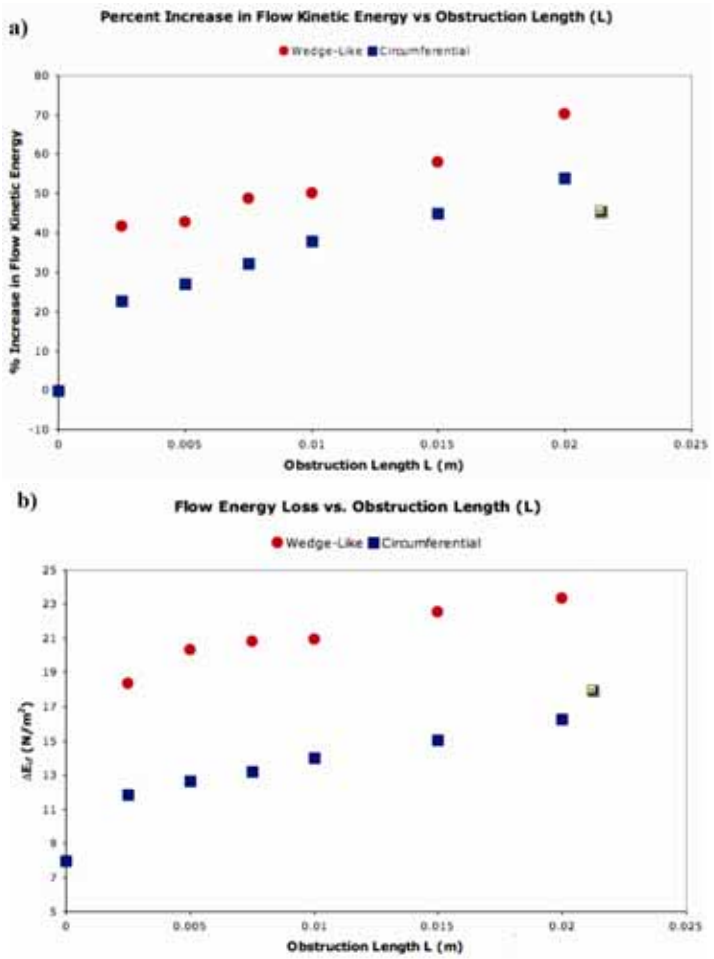


*Figure 8. (a) Percent increase in flow kinetic energy (KE) arising as a consequence of fluid crossing wedge-like (red circles) and circumferential (blue squares) obstructions of various lengths, i.e.* $\left[\frac{(KE_f - KE_i)}{KE_i} \times 100\%\right]$. *(b) Comparisons between flow energy loss terms, $\Delta E_{i,f}$, in N/m$^2$, associated with fluid crossing wedge-like (red circles) and circumferential (blue squares) obstructions of various lengths.*

$\Delta P_{i,f} = \frac{\rho}{2} V_f^2$ or $4V_f^2$, where $\Delta P_{i,f}$ is expressed in mmHg and $V_f$ in m/s. For a $\Delta P_{i,f}$ of ~ 0.2 mm Hg, the post-obstruction velocity would be ~ 0.2 m/s, a low value, but typical for systemic venous return. In the presence of energy dissipation, however,

the conversion of pressure-generated energy into energy of motion can be markedly reduced. In this case, $\Delta P$ reflects mainly flow's energy loss. In our examples, the energy loss term, $\Delta E_{i,f}$, averaged ~ 19 N/m$^2$ or ~ 0.14 mmHg, which constituted ~ 70% of the overall pressure decrease associated with the fluid reactions.

### *Phenomenological Description of Flow Energy Loss*

The calculated energy loss, $\Delta E_{i,f}$, for the various flow transitions averaged ~ 0.14 mmHg. This value should reflect a factor common to all the obstructions; e.g., the ratio of the conduit's cross-sectional area (A)-to-the obstruction's orifice area ($a$), or $\left(\frac{A}{a}\right)$. Although a fluid can speed up efficiently, it slows down inefficiently, and, in doing so, largely through viscous dissipation. Let us assume the energy loss is caused primarily by re-expansion (deceleration) of the flow, downstream from the obstruction. Using the pressure forces acting on and the momentum changes associated with the fluid mass from a vena contracta, of area $a_c$, to the distal conduit where expansion is essentially complete, of area A, the energy loss $\Delta E_{i,f}$, may be approximated by $\Delta E_{i,f} \approx \frac{\rho}{2} V_i^2 \left(\frac{A}{a_c} - 1\right)^2$ [31]. Here, $a_c = C_c\, a$, $C_c$ being the coefficient of contraction. The parameter $C_c$ is ~ 0.6 for sharp-edged, membrane-like and ~ 1.0 for elongated obstructions. By calculation, $\Delta E_{i,f}$ is 0.15 mmHg for a flow of 1 L/min, consistent with the computer-generated values.

### *Pressure and Kinetic Energy Contributions to Flow Energy Loss*

The total energy loss, $\Delta E_{i,f}$, has pressure, $(\Delta E_{i,f})_P$, and kinetic energy, $(\Delta E_{i,f})_{KE}$, contributions. Despite small overall pressure drops, the pressure term is dominant, which underscores the importance of work performed by pressure forces to overcome the impairment to flow imposed by viscous interactions. The kinetic energy component reflects changes in fluid-velocity arising from re-distribution of flow. For the types of obstructions considered, flow undergoes contraction (and hence acceleration), as it negotiates the narrowed segment of the conduit. Thus, $(\Delta E_{i,f})_{KE}$ becomes negative over the length of the conduit, i.e. $\frac{\rho}{2}\langle V^2\rangle_f$ exceeds $\frac{\rho}{2}\langle V^2\rangle_i$. It is important to note that although flow kinetic energy is gained throughout the region of obstruction, a portion of this energy is subsequently lost distal to the obstruction, as shown in Fig. 5, due to viscous dissipation. Moreover, the overall gain in kinetic energy may be considerably less than would be achieved in the absence of dissipative effects. If all the work performed by pressure forces went into changing flow's kinetic energy (i.e. no energy loss), the expression for the percent increase in kinetic energy becomes $\left[\frac{\Delta P_{i,f}}{\frac{\rho}{2} V_i^2}\right] \times 100\%$.

> ***"The treatment strategy in post-Fontan patients should be to anatomically streamline cavopulmonary passages, either by surgery or interventional catheterization procedures, in order to achieve the most gradual alterations of flow characteristics possible, and thereby materially reduce energy wastage"***

For $\Delta P_{i,f}$ ≈0.2 mmHg and a flow of 1 L/min, the increase in kinetic energy amounts to ~ 230%, compared to the ~ 50% shown in Fig. 8a.

We find the downstream kinetic energy to be greater for increasing obstruction length. This result is plausible if one considers the nature of the fluid's motion through the obstruction. As flow enters the obstruction, its velocity profile has a parabolic shape indicative of laminar flow (Figs. 3 and 4). At this point, there is a balance between pressure, viscous and inertial (acceleration) forces. Directly after entering the obstructed region, a blunt velocity profile exists. As fluid advances along the narrowed conduit, viscous factors cause fluid to slow near the walls, forming a boundary layer. Continuity demands a concomitant acceleration of the axial component of the flow in the central region of the channel. Interplay between these factors leads to narrowing of the width and elongation of the mid-portion of the velocity profile. If the obstruction is of sufficient length, flow develops a nearly parabolic velocity profile that merges readily with the distal fluid. In contrast, if the obstruction's length is short, flow exits directly into the surrounding fluid. In this case, flow advances through the contiguous reach with a more rectangular (plug-like) velocity profile, which reduces the fluid's integrated energy of motion. Although flow rate is constant throughout the conduit, kinetic energy, which depends on $\langle V^2\rangle$, may vary substantially, depending upon changes in the velocity profile. A pure rectangular profile, for example, would yield a kinetic energy one half that for a parabolic profile with an equivalent flow rate.

### *Anatomical Obstructions and Flow-Energy Loss*

The modest anatomical obstructions considered in this study provided important substrates for fluid energy loss. Elongated obstructions (20 mm) created greater energy wastage (and higher pressure drops) than highly-localized (2 mm) occlusions of equivalent flow cross-sectional area. Although both types of

impairment to flow resulted in energy dissipation from re-expansion of fluid downstream from an obstruction, extended regions of conduit narrowing may be accompanied by entrance and wall-frictional energy losses.

Since fluid cannot instantaneously turn the sharp-edged opening to an obstruction, flow is said to separate from the corners and a *vena contracta*, with area, $a_c < a$, is formed just beyond the entrance to the obstruction. However, the extra kinetic energy gained by flow within $a_c$ is partially lost due to viscous interactions within the contracted fluid stream. This causes an entrance energy loss (and pressure drop). Likewise, the greater the distance between the ends of the obstruction, the more pronounced become frictional effects, now between the moving fluid and the walls of the conduit. This boundary layer interaction leads to a wall-frictional energy loss (and pressure drop). In any case, with Fontan anatomy, an abnormal drain on systemic venous flow's energy becomes critical, since pulmonary blood flow does not receive a direct impulse from ventricular contraction or gain an additional energy supply from elastic recoil of the pulmonary arteries [23].

### *Characterization of Flow Recovery*

As flow emerges from the imposed obstructions, it encounters the more slowly moving fluid in the downstream portion of the conduit. Flow initially retains its contracted structure as it enters the larger segment of the conduit. As flow's expansion cannot be accomplished in an infinitesimal distance, it proceeds as an enlarging jet from the vena contracta to the distal portion of the conduit where uniform conditions are re-established. In the process, kinetic energy decreases (Fig. 5) and pressure increases (Fig. 6), a reflection of the Bernoulli effect. The majority of the energy loss associated with flow's expansion is due to inertial effects that are dissipated by shear stresses, now within the fluid rather than along the walls of the conduit.

Delay in flow's return to a state of uniform motion can have important implications for subsequent perfusion of the downstream fluid pathway. We found a considerable distance (about 10x conduit diameter) may be required for a flow velocity profile to achieve a distribution characteristic of the pre-obstruction state. Furthermore, plug-like velocity profiles (such as those originating from short obstructions) possess large lateral (outward) velocity gradients near the boundary of the expanding jet. This allows the central flow to diffuse more quickly toward the walls of the conduit (Figs. 3 and 4).

For the clinical cases depicted in Fig. 1, protracted delay in hemodynamic recovery would imply disordered flow enters the branch pulmonary arteries. This condition would exacerbate the kinetic energy loss encountered as flow undergoes the acute change in angulation required to perfuse the lungs [9]. Another consideration is the development of flow stagnation (Figs. 3, 4 and 7), either proximal or distal to an obstruction. Impaired forward flow in the shadow of a wedge-like occlusion, for example (Fig. 1A), could lead to disproportionate hepatic venous return to the branch pulmonary arteries; a condition that has been implicated in the development of pulmonary arteriovenous fistula [32]. Regions of flow stasis also predispose to thrombus formation in post-Fontan patients, since they often possess an underlying coagulation factor deficiency [33-34].

### Conclusions

In a passively perfused fluid system, important flow energy can be lost across anatomically-significant obstructions, in the presence of small overall pressure change. This process is relevant in the low-velocity, sometimes tortuous cavopulmonary pathway of post-TCPC patients. Using a computer-based description of steady fluid flow through an obstructed conduit, we identified energy-depleting flow disturbances characterized by prominent regions of flow stagnation and flow reversal, with pressure drops averaging only ~ 0.2 mm Hg. Approximately 70% of these pressure changes were found to be due to flow energy dissipation. The treatment strategy in post-Fontan patients should be to anatomically streamline cavopulmonary passages, either by surgery or interventional catheterization procedures, in order to achieve the most gradual alterations of flow characteristics possible, and thereby materially reduce energy wastage. We believe that maintaining an energy-efficient cavopulmonary circulation will undoubtedly improve long-term clinical outcome of modified Fontan patients.

### Acknowledgments

We thank Comsol Multiphysics Corporation, Burlington, MA, for their valuable technical support.

### References

1. Thorax. 1971; 26:240-248. Surgical repair of tricuspid atresia. Fonan F, Baudet E.

2. Circulation. 1998; 98:1099-1107. Predictors of early and late-onset supraventricular tachycardia after Fontan operation. Durongpisitkul K, Co-burn JP, Cetta F, Offord KP, Slezak JM, Puga FJ, Schaff HV, Danielson GK, Driscoll DJ.

3. Circulation. 1992; 85:469-496. Five to fifteen-year follow-up after Fontan operation. Driscoll DJ, Offord KP, Feldt R, Schaff HV, Puga FJ, Danielson GK.

4. J Thorac Cardiovasc Surg. 1998; 96:682-695. Total cavopulmonary connection a logical alternative to atriopulmonary connection

for complex Fontan operations. Experimental studies and early clinical experience. de Leval MR, Kilner P, Gewillig M, Bull C.

5. Ann Thorac Surg. 1991; 52:180-196. Total cavopulmonary anastomosis vs. conventional modified Fontan procedure. Pearl JM, Laks H, Stein DG, Drinkwater DW, George BL, Williams RG.

6. Circulation. 1995; 91:2943-2947. Modification of the Fontan procedure: superior vena cava to left pulmonary artery connection and inferior vena cava to right pulmonary artery connection with adjustable atrial septal defect. Laks H, Ardehali A, Grant PW, Permut L, Ahaon A, Kuhn M, Isabel-Jones J, Galindo A.

7. Circulation. 1998; 98:2873-2882. In vivo evaluation of Fontan pathway flow dynamics by multidimensional phase-velocity magnetic resonance imaging. Be'eri E, Maier SE, Landzberg MJ, Chung T, Geva T.

8. Pediatr Cardiol. 2001; 22:110-115. Pressure loss from flow-enery dissipation: relevance to Fontan-type modifications. Ascuitto RJ, Kydon DW, Ross-Ascuitto NT.

9. Pediatr Cardiol. 2003; 24:249-258. Streamlining fluid pathways lessens flow-energy dissipation: relevance to atriocavopulmonary connections. Ascuitto RJ, Kydon DW, Ross-Ascuitto NT.

10. J Thorac Cardiovasc Surg. 1996; 111:505-513. Use of computational fluid dynamics in the design of surgical procedures: application to the study of competitive flows in cavopulmonary connections. de Leval MR, Dubini G, Migliavacca F, Jalali H, Camporini G, Redington A, et al.

11. Circulation. 1987; 76:III53-III60. Modifications of the Fontan operation applicable to patients with left atrioventricular valve atresia or single atrioventricular valve. Puga FG, Chiavarelli M, Hagler DJ.

12. Pediatr Cardiol. 2004; 25:472-481. Systemic-to-pulmonary collterals: A source of flow energy loss in Fontan physiology. Ascuitto RJ, Ross-Ascuitto NT.

13. Ann Thorac Surg. 1999; 68:1384-1390. Toward designing the optimal total cavopulmonary connection: An in vitro study. Ensley A, Lych P, Chatzimavroudis GP, Lucas C, Sharma S, Yoganathan AP.

14. Heart. 1999; 81:67-72. Pulmonary and caval flow dynamics after total cavopulmonary connection. Houlind K, Stenbog EV, Sorensen KE, Emmersen K, Hansen OK, Rybro L, Hjortdal VE.

15. J Biomech. 1995; 117:423-429. Hemodynamics of the Fontan connection: An in-vitro study. Kim YH, Walker PG, Fontaine AA, Panchal L, Ensley AE, Oshinski J, Sharma S, Ha B, Lucas CL, Yoganathan AP.

16. J Thorac Cardiovasc Surg. 1999; 117:697-704. Fluid dynamic comparison of intraatrial and extracardiac total cavopulmonary connections. Lardo AC, Webber SA, Friehs I, del Nido PJ, Cape EG.

17. J Biomed Eng. 1993; 15:303-307. Flow studies on atriopulmonary and cavopulmonary connections of the Fontan operations for congenital heart defects. Low H, Chew Y, Lee C.

18. J Am Coll Cardiol. 1996; 27:124-126. In vivo flow experiments for determination of optimal geometry of total cavopulmonary connection for surgical repair of children with functional single ventricle. Sharma S, Goudy S, Walker P, Panchal S, Ensley A, Kanter K, Tam V, Fyfe D, Yoganathan A.

19. J Thorac Cardiovasc Surg. 2003; 126(4):1040-1047. Computational fluid dynamics in the evaluation of hemodynamic performance of cavopulmonary connections after the Norwood procedure for hypoplastic left heart syndrome. Bove El, de Leval MR, Migliavacca F, Guadagni G, Dubini G.

20. J Biomech. 1996; 29:111-121. A numerical fluid mechanical study of repaired congenital heart defects: Application to the total cavopulmonary connection. Dubini G, de Leval M, Pietrabissa R, Montevecchi F, Fumero R.

21. J Biomech Eng. 2001; 123:317-324. Noninvasive fluid dynamic power loss assessments for total cavopulmonary connections using the viscous dissipation function: A feasibility study. Healy TM, Lucas C, Yoganathan AP.

22. Circulation. 1995; 92(9):II322-326. Comparison by computerized numeric modeling of energy losses in different Fontan connections. Van Haesdonk JM, Mertens L, Sizaire R, Montas G, Purnode B, Daenen W, et al.

23. Heart. 1999; 82:294-299. Instantaneous pressure-flow velocity relations of systemic venous return in patients with univentricular circulation. Kaulitz R, Bergman P, Lihmer I, Paul T, Hausdorf G.

24. Rev Argent Cardiol. 1996; 64:379-388. Interventional cardiac catheterization in patients with Fontan circulation. Kreutzer J.

25. J Thorac Cardiovasc Surg. 1997; 117:1032-1041. The nature of flow in the systemic venous pathways measured by magnetic resonance blood tagging in patients having the Fontan operation. Fogel MA, Weinberg PM, Hoydu A, Hubbard A, Rychik J, Jacobs M, et al.

26. Artif Organs. 2000; 24:946-952. Particle image velocimetry analysis of the flow field in the total cavopulmonary connection. Grigioni M, Amodeo A, Daniele C, D'Avenio G, Formigari R, DiDonato RM.

27. JACC. 1993; 21:123-131. Postoperative pulmonary flow dynamics after Fontan surgery: assessment with nuclear magnetic resonance velocity mapping. Rebergen SA, Ottenkamp J, Doornbos J, van der Wall EE, Chin JGJ, de Roos A.

28. Ann Thorac Surg. 2001; 71:889-898. In vivo flow dynamics of the total cavopulmonary connection from three-dimensional multislice magnetic resonance imaging. Sharma S, Ensley AE, Hopkins K, Chatimavroudis GP, Healy TM, Tam VKH, Kanter KR, Yoganathan AP.

29. IEEE Trans Biomed Eng. 1999; 46:393-399. Computational fluid dynamics and magnetic resonance analysis of flow distribution between the lungs after total cavopulmonary connection. Migliavacca F, Kilner PG, Pennati G, Dubini G, Pietrabissa R, Fumero R, de Leval MR.

30. Comsol Multiphysics Conference Proceedings. 2005 pg. 411-416. A Computational Investigation of Flow-Mechanical Energy Loss: Relevance to the Total Cavopulmonary Connection. Wiesman JP, Ross-Ascuitto NT, Gaver DP, Ascuitto RJ.

31. Viscous flow in pipes-In: Fundamentals of Fluid Mechanics 4th Edition John Wiley & Sons, 2002, New York, pp 443-531. Munson BR, Young DF, Okiiski TH.

32. Ann Thorac Surg. 2005; 80:1597-1603. Incorporation of the Hepatic Veins Into the Cavopulmonary Circulation in Patients With Heterotaxy and Pulmonary Arteriovenous Malformations After a Kawashima Procedure. McElhinney DB, Kreutzer J, Lang P, Mayer JE, del Nido PJ, Lock JE.

33. Lancet. 1990; 336:1087-1090. Coagulation factor abnormalities as possible thrombotic risk factors after Fontan operations. Cromme-Dijkhuis AH, Henkens CMA, Bijleveld CMA, Hillege HL, Born VJJ, Van der Meer J.

34. J Thorac Cardiocasc Surg. 1997; 113:989-993. Coagulation factor abnormalities after Fontan procedure and its modifications. Jahangiri M, Shore D, Kakkar V, Lincoln C, Slinebourne E.

~CCT~

***Corresponding Author***

*Robert J. Ascuitto, PhD, MD*
*Division of Pediatric Cardiology*
*Departments of Pediatrics and Physics*
*Tulane University Health Sciences Center*
*1430 Tulane Avenue*
*New Orleans, LA 70112 USA*

*Tel: (504) 884-0660*

*Joshua P. Wiesman, MS*
*Department of Biomedical Engineering*
*Tulane University School of Engineering*

*Donald P. Gaver , PhD*
*Department of Biomedical Engineering*
*Tulane University School of Engineering*

*Nancy T. Ross-Ascuitto, MD*
*Departments of Pediatrics*
*Tulane University Health Sciences Center*

**Moving?** To continue receiving Congenital Cardiology Today, send your new address to Moving@CCT.bz

# THE WORLD LOSES A GIFTED PEDIATRIC CARDIOLOGIST, PATHOLOGIST AND PHILOSOPHER

*By Richard Van Praagh, MD*

Stella Van Praagh, MD was a world renowned pediatric cardiologist and pathologist of Children's Hospital Boston and Harvard Medical School who died following a very brief illness on June 3rd, 2006. The author of more than 100 scientific publications on pediatric cardiology, congenital cardiac pathology, and congenital heart surgery, she played a key role in developing the diagnostic approach to the understanding of complex heart disease in infants and children that is now used worldwide. In addition, Dr. Stella Van Praagh clarified the pathologic anatomy and embryology of many different forms of structural heart disease in infants and children, which led in turn to more accurate diagnosis and more successful surgical management.

Born in Rethymnon, Crete, Greece and née Stella Zacharioudaki, she graduated from the School of Medicine of the University of Athens, Greece in 1952. Following 9 years of postgraduate work, almost all in the USA and Canada, she was invited to join the Pediatric Cardiology staff of the Buffalo Children's Hospital, Buffalo, NY, in 1962. In the same year, she married Richard Van Praagh, MD, beginning a lifelong love affair and professional collaboration. Richard and Stella were a team of investigative pediatric cardiologists and pathologists, who were invited to join the staff of Children's Hospital Boston in 1965 and have worked there ever since. Richard was Stella's first teacher of a then new anatomic and developmental approach to the diagnostic understanding of congenital heart disease. In recompense, Stella has been teaching Richard ever since. As Stella once said with a twinkle in her eye, "Dickie, you and I have proved that husbands and wives really can work together."

The family of Drs. Stella and Richard Van Praagh consists of 3 children — Andrew, Helen (who died in 2001), and Alexander — plus 5 (soon to be 6) grandchildren. In addition to being a superb clinician and medical scientist, she was also a remarkable cuisinière. Her baklava and bread were legendary. Adored by her patients and her many students and colleagues, she was a second mother to many of them.

In addition to modern Greek, Dr. Stella Van Praagh was also conversant with Byzantine Greek and ancient Greek. Aristotle had written that the human heart normally has three ventricles. ("Everyone" now knows that the human heart normally has only two ventricles.) The problem of Aristotle's "triventricular" heart had remained unresolved for the past twenty-two hundred years. Consequently, Dr. Stella Van Praagh translated Aristotle's ancient Greek text, to check on the accuracy of the translation by Oxford classicists, and to correct their errors. Suffice it to say that her accurate translation proved to be an important part of the solution of this long-standing mystery.

At the urging of friends, Dr. Stella Van Praagh led an ancient Greek studies group in Wellesley, fondly known as the Mythology Club. She was that very rare combination: a physician — philosopher. As these words are being written, the Mythology Club is meeting — to celebrate the life of Dr. Stella Van Praagh.


Many friends and colleagues sensed that there was something very different about Dr. Stella. Some saw her as a visionary. Others were awed by her great inner strength and her fearless integrity. She was also modest, self-effacing, and always anxious to help others. The last act of her life was to make a hot dinner, that only she in our family knows how to make (pasticcio), and she took it to her son Andrew's home because Catherine, Andrew's wife, is now full-term and awaiting delivery. Abigail, Andrew and Catherine's first child, loves pasticcio.

Dr. Stella Van Praagh was the embodiment of what Socrates and Plato called virtue. She had the courage and the integrity always to call it as she saw it, no matter how difficult or unpopular that might be.

Dr. Stella Van Praagh wore many hats, all of them well: cardiologist, pathologist, philosopher, wife, mother, grandmother, incomparable friend, and wise counselor.

~CCT~

# SEARCHING FOR AND MENDING BROKEN HEARTS IN MONGOLIA

*By Kirk A. Milhoan, MD, PhD; Kimberly D. Milhoan, MD; Ariuntsatsral Erdenebileg, MD*

During the last two weeks of October 2005, thirty people from all across the United States traveled to Ulaan Baatar, Mongolia to search for children with congenital heart disease and begin a new chapter in pediatric cardiac surgery there.

***Team Photo:*** *Mending the Broken Hearts Team: From left to right; Back: Dr. Galsumiya, Rita Browning, Bart Hensler, Kim Milhoan, John Kupferschmid, David Bush, Gail Fox. Middle: Dr. Byambasuren, Dr. Tsegeenjav, Dr. Baasanjav, Tammy Amidon, Dr. Bolormaa, Dr. Arriuntsatsral, Nelia Doegenes Front: Bayarjavkhlan Browning, Kirk Milhoan and Dr. Boldsaikhan.*

During the first week, a large-scale screening, called *Searching for the Broken Hearts*, was carried out in five Ulaan Baatar district hospitals and one Mongolian rural hospital by the volunteers from For Hearts and Souls, a non-profit medical mission organization, in cooperation with many Mongolian physicians and nurses. Children were evaluated with vital signs and complete cardiac exams by physicians. Those children who had murmurs that were thought to be pathologic were further evaluated by a pediatric cardiologist. If the physical exam was consistent with a pathologic condition, the child then underwent a complete echocardiogram, with an Acuson Cypress machine. Over 1500 children were evaluated and over 300 echocardiograms were performed. The fact that over twenty percent of the children underwent echocardiograms demonstrates the heavy representation of children who had been previously diagnosed with congenital heart disease or had a history of a murmur in the screened population.

This screening was the third such large-scale endeavor since September 2003. However, Kirk Milhoan, MD, PhD, had made six previous trips to Ullaan Baatar, in conjunction with Samaritan Purse's Children's Heart Project, beginning in December 2000. The purpose of his first trip was to train Mongolian pediatric cardiologists on the use of color doppler echocardiography, performed with a Hewlett Packard 1000 donated by Samaritan's Purse (SP), as this technique had not been previously used in Mongolia. The purpose of his subsequent trips has been to:

1) identify children with operable congenital heart disease, before they become inoperable or die from their heart disease;
2) increase awareness among Mongolian physicians of the need for children thought to have congenital heart disease to receive complete evaluation early in life to make early repair possible before irreversible pulmonary obstructive disease develops;
3) provide continuing medical education for Mongolian pediatric cardiologists and cardiac surgeons on diagnosis and management of children with congenital heart disease; and
4) raise awareness of the need for further development of the medical infrastructure to increase the ability to care for vulnerable children with congenital heart disease in Mongolia.

The magnitude of the need in Mongolia inspired him to organize the large scale screenings in conjunction with For Hearts and Souls, an organization he started with his wife, Kimberly Milhoan, MD. Other locations visited on these large-scale trips have been the rural Mongolian provinces of Darkhan, Bulgan, Erdenet, and Tuv. The total number of children screened to date exceeds five-thousand.

Since June 2000, SP's Children's Heart Project has brought over seventy Mongolian children identified during these screenings to the U.S. and Canada for cardiac surgery. The current state of pediatric cardiac surgery in Mongolia consists of ether anesthesia with hypothermic circulatory arrest without cardiac pulmonary bypass. The Mongolian cardiothoracic surgeons usually will not operate on children younger than age three. The cardiac lesions they will attempt are atrial septal defects (ASD) and ventricular septal defects (VSD). These limitations are due in part to lack of medical team training, operating room equipment, intensive care unit facilities, and financial resources. Mongolian hospitals, who receive very limited

government financial assistance, are legally prohibited from charging children's families for medical care, although they can charge adult patients. Thus, bypass procedures are traditionally only performed on adults that are able to provide for the cost of the bypass circuit and the other consumables for the surgery. The operative mortality for pediatric cardiac surgery in Mongolia is a difficult figure to obtain, but is estimated to be between 10 and 50%.

These screenings have obviously revealed many more children in need of cardiac surgery than could be handled by sending them to the U.S. or Canada. The goal of the Mending the Broken Hearts team was to bring pediatric cardiac surgery with cardiac bypass to Mongolia, working side by side with the Mongolian physicians and nurses. This project was co-sponsored by Samaritan's Purse Children's Heart Project, World Medical Mission (the medical arm of Samaritan's Purse) and For Hearts and Souls. Close to $500,000 worth of

***ICU:*** *Cathy Woodward teaching Mongolian nurses on post-operative bedside care in the Surgical Intensive Care Unit at the Shastin Memorial 3rd Hospital in Ulaan Baatar*

equipment, including a cardiac bypass machine, an anesthesia machine, monitors for the intensive care unit, and consumables needed to perform cardiac surgeries, was sent and given to Mongolia. The team consisted of a pediatric cardiothoracic surgeon, John Kupferschmid, MD; a pediatric cardiac anesthesiologist, Kimberly Milhoan, MD; a pediatric cardiac

***Hypothermic circulatory arrest:*** *Patient is wrapped in ice and cooled to 28 C prior to closure of an ASD using hypothermia alone. In the background a nurse can be seen functioning as the ventilator for this patient who is being maintained on ether anesthesia.*

perfusionist, Bart Hensler, CCP; a pediatric cardiac intensivist, Minette Son, MD; pediatric cardiologists, David Bush, MD, PhD and Kirk Milhoan, MD, PhD; a pediatric nurse practitioner, Cathy Woodward, PNP; a cardiac scrub nurse, Gail Fox, RN; four pediatric cardiac intensive care nurses, Nelia Doegenes, RN, Cindy Eckhardt, RN, Tammy Amidon, RN, and Debi Lammert, RN; and two biomedical technicians, Jim Moore and Todd Poore. The Mongolian team consisted of four pediatric cardiologists, four cardiothoracic surgeons, and two anesthesiologists.

The team performed eight cardiac surgeries, four of them utilizing cardiac bypass, in four days. The first ever pediatric cardiac surgery with cardiac bypass performed in Mongolia was on an 11-year-old female with a VSD who had received a pulmonary artery band from an Australian team that had visited in 1998. The VSD was closed and the pulmonary band was removed. The other three bypass cases were ASD closure in two symptomatic patients (a 3-year-old and a 13-year-old)

***First pediatric bypass patient:*** *Dr. Milhoan with Munkhdelger, the first patient to undergo pediatric cardiac surgery in Mongolia with cardiac bypass.*

***OR Nurses:*** *Gail Fox, an OR nurse from San Antonio, with a group of Mongolian OR nurses.*

***First balloon septostomy in Mongolia:*** *Echo-guided balloon atrial septostomy by two Mongolian pediatric cardiologists. Dr. Arriuntsatsral is performing the echocardiogram while Dr. Bolormaa is performing the septostomy. The balloon can be seen partially inflated in the left atrium.*

and aortoplasty in a 15-year-old with supravalvar aortic stenosis. The four non-bypass procedures were ligation of PDAs in three patients with very large and symptomatic ducts and one pulmonary artery band in a 2-year-old child with a very large VSD. It was deemed too high risk to close this last child's VSD given the state of post-operative intensive care. All eight children did very well post-operatively. None remained intu-

***First pediatric bypass surgery:*** *Operating room at the Shastin Memorial 3rd Hospital during the first pediatric heart surgery in Mongolia utilizing cardiac bypass.*

***Anesthesiologist and surgeons working together:*** *Drs. Milhoan and Kupferschmid working side by side with Mongolian physicians during pediatric cardiac surgery.*

bated overnight and all were discharged from the hospital prior to the team leaving Mongolia. The team was also able to assist two Mongolian pediatric cardiologists in performing, with echo guidance, the first two atrial septostomies performed in Mongolia, one on an infant with transposition of the great arteries and the other on a neonate with tricuspid with a restrictive ASD. Although the procedures were successful, unfortunately both infants died within two months from complications of their congenital heart defects.

The Searching for and Mending the Broken Heart teams from the U.S. plan to return to Mongolia in September 2006.

**Acknowledgments**

The authors would like to thank: Medical Director of the Shastin Memorial 3rd Hospital: Dr. Batsereeden; Vice Minister of Health: Dr. Enkhbat, Director of the Maternal and Child Health Research Center: Dr. Erkhembaatar and Cardiothoracic surgeons from the Shastin Memorial 3rd Hospital: Drs: Baasanjav, Boldsaikhan, and Tsegeenjav for their support of this project.

**~CCT~**

***Corresponding Author***

*Kirk A. Milhoan, MD, PhD*
*Medical Director*
*For Hearts and Souls*
*2850 Lakehills St.*
*San Antonio, TX, 78251 USA*
*Tel: (210) 292-0206*

*kirk@forheartsandsouls.org*

*www.forHeartsandSouls.org*

*Kimberly D. Milhoan, MD*
*Assistant Professor*
*University of Texas Health Sciences Center San Antonio*
*Department of Anesthesiology*
*San Antonio, TX USA*

*Milhoan@uthscsa.edu*

*Arriuntsatsral Erdenebileg, MD*
*Pediatric Cardiologist*
*Maternal and Child Health Research Center*
*Ulaan Baatar, Mongolia*

*tsatsrale@yahoo.com*

**CONGENITAL CARDIOLOGY TODAY**


(ISSN 1554-7787-print; ISSN 1554-0499-online)
*Published monthly. All rights reserved*

***Publishing Management***
*Tony Carlson, Founder*
*TCarlsonmd@gmail.com*
*Richard Koulbanis, Publisher & Editor-in-Chief*
*RichardK@CCT.bz*
*John W. Moore, MD, MPH, Medical Editor/ Editorial Board*
*JWMoore@CCT.bz*

# iE33 – INTELLIGENT ECHO FOR EVERY STAGE OF LIFE


*Live 3D Echo .*


*PureWave Crystal Technology..*

In the last 20 years, there has been a revolution in caring for children with congenital heart disease. Thanks to advances in diagnostics, surgery and treatment, many of these children are living into adulthood and enjoying active lives. With dedicated pediatric cardiology capabilities, the iE33 echo system answers your need for high-performance, non-invasive diagnostic imaging for these patients.

From fetal echo to mature adult, the iE33 system supports the assessment of congenital heart disease through every stage of life and provides new diagnostic information that is changing patient management. Everything about the system is designed to meet the specific needs of pediatric cardiology. Unique ergonomic features make it possible to successfully image the tiniest premie or the largest teenager in many different environments. Pediatric analysis follows your workflow. And advanced technologies provide best-in-class 2D imaging and Live 3D Echo and give clinicians and surgeons structural information to make decision making more efficient and outcomes more effective.

***Pediatric cardiology imaging capabilities from fetal echo up to the mature adult for complete Congenital Heart Disease assessment with analysis capabilities that looks at inflow and outflow of information within the pediatric heart. Listen to the Podcast: http://tinyurl.com/s42k6***

A full complement of cardiac transducers, including pediatric and adult TEEs, enables you to image a complete range of patient types – regardless of age, disease state or body composition.

In addition, a unique analysis package truly follows the patient the way you do – so you don't have to fit your requirements into an analysis package designed for adult echocardiography.

The biggest breakthrough in transducer material in 40 years, PureWave crystal technology provides significantly better acoustic properties for a radical leap forward in 2D image quality.

Dedicated to your pediatric cardiology clinical and workflow requirements, our commitment goes beyond the system and its technologies. Global educational programs, outstanding service and worldwide centers of excellence help you to get the most out of your system every day.

***Pediatric echo from Philips…***
***it just makes sense.***

**FOR MORE INFORMATION**

Philips Medical Systems
22100 Bothell Everett Highway
Bothell, WA 98021
+1 (425) 487 7000
1 (800) 285-5585

www.medical.philips.com/ultrasound

PHILIPS